Boundary Intensification of Vertical Velocity in a β-Plane Basin

JOSEPH PEDLOSKY* AND MICHAEL A. SPALL

Department of Physical Oceanography, Woods Hole Oceanographic Institution, Woods Hole, Massachusetts

(Manuscript received 28 September 2004, in final form 13 June 2005)

ABSTRACT

The buoyancy-driven circulation of simple two-layer models on the β plane is studied in order to examine the role of beta in determining the magnitude and structure of the vertical motions forced in response to surface heating and cooling. Both analytical and numerical approaches are used to describe the change in circulation pattern and strength as a consequence of the planetary vorticity gradient. The physics is quasigeostrophic at lowest order but is sensitive to small nonquasigeostrophic mass fluxes across the boundary of the basin. The height of the interface between the two layers serves as an analog of temperature, and the vertical velocity at the interface consists of a cross-isopycnal velocity, modeled in terms of a relaxation to a prescribed interface height, as well as an adiabatic representation of eddy thickness fluxes parameterized as lateral diffusion of interface displacement. In the numerical model the lateral eddy diffusion of heat is explicitly represented by a resolved eddy field. In the plausibly more realistic case, when the lateral diffusion of buoyancy dominates the diffusion of momentum, the major vertical velocities occur at the boundary of the basin as in earlier *f*-plane studies. The effect of the planetary vorticity gradient is to intensify the sinking at the western wall and to enhance the magnitude of that sinking with respect to the *f*-plane models. The vertical mass flux in the Sverdrup interior exactly balances the vertical flux in the region of the strong horizontal transport of the western boundary current, leaving the *net* flux to occur in a very narrow region near the western boundary tucked well within the western boundary current. On the other hand, if the lateral diffusion of heat is arbitrarily and unrealistically eliminated, the vertical mass flux is forced to occur in the interior. The circulation pattern is extremely sensitive to small net inflows or outflows across the basin perimeter. The cross-basin flux determines the interface height on the basin's eastern boundary and affects the circulation pattern across the entire basin.

1. Introduction

In a series of recent papers (Spall 2003a, 2004; Pedlosky 2003) the buoyancy-driven circulations of relatively small ocean basins were examined, and these studies demonstrated the tendency for the major sinking (or upwelling) of fluid to occur along ocean boundaries where the dissipative interaction with the boundary allows the vorticity and thermal anomalies produced by the vertical motion to be efficiently dissipated. The scales of the basins were considered small enough so that the planetary vorticity gradient, the β effect, could be ignored. It is natural to wonder what effect the removal of that simplification might have on the structure of the sinking given the well-known tendency of the beta effect to intensify the horizontal motion in the western part of the basin and because of the relevance of these ideas to the large-scale thermohaline circulation for which the β effect is important. This is especially of interest since the sinking or rising in the narrow boundary layers in the *f*-plane models is in direct proportion to the lateral tangential velocity just external to these regions of strong vertical motion. In general, although much attention is often focused on the upwelling component of the thermohaline circulation and its relation to mixing, instead we here emphasize the strong role of mixing in determining the location and structure of the sinking branch of the circulation. This

* Woods Hole Oceanographic Institution Contribution Number 11295.

Corresponding author address: Joseph Pedlosky, Woods Hole Oceanographic Institution, Dept. of Physical Oceanography, Clark 363, MS #21, Woods Hole, MA 02543.
E-mail: jpedlosky@whoi.edu

study is motivated by a range of applications in which buoyancy forcing and the beta effect are important, including high-latitude polar seas, marginal seas, and basin-scale thermohaline circulations.

Several recent studies have explored the role of boundaries and boundary enhanced diapycnal mixing in the thermohaline circulation (Marotzke 1997; Samelson 1998; Huck et al. 1999; LaCasce 2004). The primary difference between those studies and the present one is one of position in parameter space. We have chosen to focus on the regime in which viscosity is small and surface buoyancy anomalies are weakly damped by air–sea exchange. In physical terms, this corresponds to the limit in which the viscous boundary layer is thin compared to the lateral diffusive length scale and the distance a baroclinic Rossby wave can propagate before it is damped is of the same order as the basin width. The first limit (small friction) eliminates the Munk layer and results in the thermal diffusive layer playing a key role in the net vertical and horizontal motion in the basin. The second limit (weak damping of anomalies) allows for significant buoyancy-forced meridional flow in the interior of the basin. Most general circulation models of the thermohaline circulation are of low horizontal resolution and have been run with the viscous boundary layer of the same order of magnitude as the diffusive boundary layer width, in other words, with an active Munk layer. They also typically use an air–sea damping sufficiently strong so that Rossby waves cannot propagate far from the eastern boundary, particularly at high latitudes. As a consequence for those studies, the flow in the interior is constrained to be primarily zonal and the meridional transports occur in viscous boundary layers. Also, we do not specify the boundaries as regions of enhanced importance, a priori, but they do emerge as a region of enhanced vertical motion as a result of the dynamics of the resolved boundary layers.

To examine this question in the simplest context we consider a two-layer model whose density interface (Fig. 1) represents the buoyancy field. The vertical motion of interest at the interface is modeled as a cross-isopycnal flux across the interface parameterized in terms of the deviations of the interface from a specified height. This specified, spatially variable height of the interface plays the role of an external heating or cooling of the basin's surface and the resulting horizontal circulation determines the structure of the buoyancy field and the vertical flux of mass. In addition, a lateral diffusion of thickness is explicitly included in the analytical model. This contribution is consistent with the Gent and McWilliams (1990) representation of *adiabatic* eddy fluxes of thickness by an unresolved baroclinic

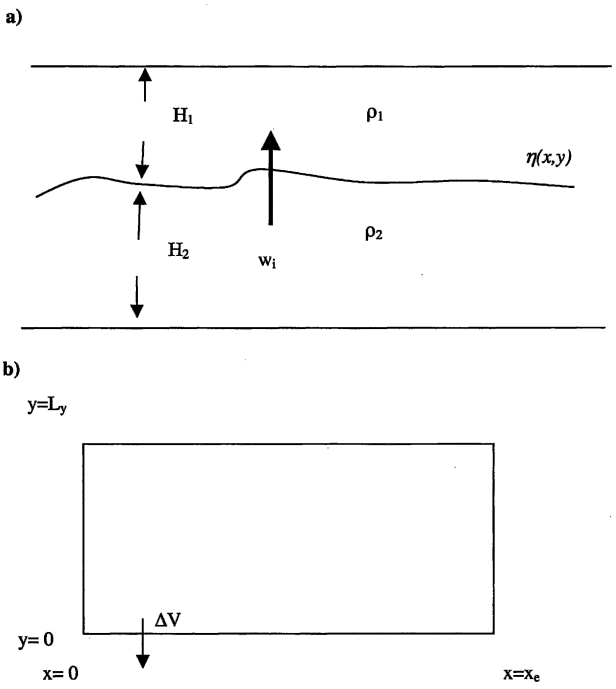

FIG. 1. The two-layer model used in this study. Each layer consists of fluid of constant and specified density but thermodynamic processes allow cross-interface fluxes. The model is shown in (a) cross section and in (b) plane view.

eddy field. However, the diffusive term could also be interpreted as a locally *nonadiabatic* process of submesoscale mixing and this would be especially apt in the narrow boundary layers near the basin boundaries where adiabatic mesoscale eddy fluxes must vanish. The motion in the basin is also driven by a small and specified flux of mass across the perimeter of the basin.

We derive a quasigeostrophic model in section 2 in its linear form and describe the boundary layer structure to be expected in the analytical treatment of the model. The boundary layer structure is rather complex; the closure of the vertical and horizontal circulations occur in different branches of the flow. Furthermore, the structure itself strongly depends on the parameters of the model. We attempt to describe the circulation in a range that we feel is the most robust. The results of the linear model are described in detail in section 3, and the overall predictions of the model are compared with planetary geostrophic and nonlinear numerical calculations in section 4 where it is shown that the qualitative features of the linear model are good predictors of the planetary geostrophic and, nonlinear, eddy-rich primitive equation solutions. In section 5 we summarize our results and speculate on their oceanographic significance.

2. The model

a. Formulation

The model is shown in Fig. 1. Two layers of slightly different density are separated by an interface whose elevation above its rest level is $\eta(x, y)$, where x is a coordinate to the east and y is a coordinate to the north. The rest thicknesses of each layer H_1 and H_2 are chosen to be equal (H). The flow is driven by buoyancy forcing alone and in the absence of topography in our model the resulting circulation is purely baroclinic. We represent the baroclinic horizontal velocity as

$$\mathbf{u} = \mathbf{u}_1 - \mathbf{u}_2. \tag{2.1}$$

The linear equations of motion of the model are, for the baroclinic mode, similar to the model used by Gill (1982):

$$fu = g'\eta_y + A\nabla^2 v, \tag{2.2a}$$

$$-fv = g'\eta_x + A\nabla^2 u, \quad \text{and} \tag{2.2b}$$

$$u_x + v_y = 2\frac{w_i}{H}. \tag{2.2c}$$

In (2.2a) and (2.2b) $f = f_o + \beta y$, A is the coefficient of momentum mixing and w_i is the cross-isopycnal velocity. In the linear model it is also the vertical velocity. Note that a positive w_i represents a heating of the model since dense fluid is transformed into lighter fluid.

The key feature of the model is the parameterization of the vertical velocity at the interface. It is represented as a cross-isopycnal velocity, given in terms of the interface displacement and a vertical velocity driven by a diffusion of thickness.

We choose the following parameterization with the character of a continuous model in mind, namely,

$$w_i = \gamma(\eta - h) - \kappa\nabla^2\eta. \tag{2.3}$$

The vertical velocity is thus driven by two processes. The first term on the right-hand side of (2.3) produces a velocity when the interface height departs from a specified field $h(x, y)$. The relaxation to this field occurs with an inverse time scale γ. The field h represents a cooling process if h exceeds η since then it tends to drive less dense fluid into the lower layer where it becomes more dense. We imagine that h is a representation of the direct effect of atmospheric cooling on the temperature of the fluid, so the first term on the right-hand side of (2.3) is our parameterization of vertical mixing processes that tend to restore the temperature to the equilibrium value determined by the atmospheric forcing. The second term on the right-hand side of (2.3) is a lateral diffusion of interface height and, in this model, parameterizes the lateral diffusion of buoyancy produced by unresolved eddy processes. The coefficient of lateral mixing is κ. In the interior of the fluid, away from the boundaries, we interpret this diffusion of thickness as a way to model the result of an unresolved eddy field and its adiabatic flux of thickness. Near the boundaries, and in particular in the boundary layers, we think of the same process as representing a small-scale nonadiabatic mixing process. Clearly, our simple model does not really distinguish between them and this interpretation is heuristic rather than rigorous.

We introduce the following nondimensional scaling indicating nondimensional variables with primes:

$$(x, y) = L(x', y'), \tag{2.4a}$$

$$(u, v) = U(u', v'), \tag{2.4b}$$

$$w_i = U\frac{H}{L}w_i', \tag{2.4c}$$

$$h = h_o\theta(x, y), \tag{2.4d}$$

$$\eta = \frac{f_o UL}{g'}\eta', \quad \text{and} \tag{2.4e}$$

$$U = \frac{g'h_o}{f_o L}. \tag{2.4f}$$

The last relation fixes the scaling for the horizontal velocity in terms of the amplitude of the applied buoyancy forcing. Using this scaling the equations can be written in nondimensional form as (after dropping the primes on dimensionless variables):

$$fu = \eta_y + b\delta_m^3\nabla^2 v, \tag{2.5a}$$

$$-fv = \eta_x + b\delta_m^3\nabla^2 u, \tag{2.5b}$$

$$u_x + v_y = 2w_i, \quad \text{and} \tag{2.5c}$$

$$w_i = b\left(\frac{\eta - \theta}{\delta_T} - \delta_K\nabla^2\eta\right). \tag{2.5d}$$

The following parameters are key:

$$\delta_m = (A/\beta)^{1/3}/L, \tag{2.6a}$$

$$\delta_T = \frac{\beta L_d^2}{\gamma L}, \tag{2.6b}$$

$$\delta_K = \frac{\kappa}{\beta L_d^2 L}, \tag{2.6c}$$

$$b = \frac{\beta L}{f_o}, \quad \text{and} \tag{2.6d}$$

$$L_d^2 = \frac{g'H}{f_o^2}. \tag{2.6e}$$

The first three parameters are measures of length. They are the nondimensional Munk boundary layer thickness, a thermal boundary scale, and a diffusion scale.

Each is scaled with the basin scale L. The thermal boundary scale δ_T is a measure of how far a long Rossby wave can travel westward before it is damped by the relaxation process whose damping rate is γ. The diffusion scale measures the ratio of the time it takes a long Rossby wave to cross the basin to a diffusion time on the scale of the basin. We will consider a parameter regime in which the Munk scale and the diffusion scale are small. The thermal boundary scale may be of order 1 or less. The β-plane parameter b is considered small so that quasigeostrophic β-plane dynamics will be valid. However, we are also interested in basins in which the meridional extent is sufficiently large so that the explicit variation of f becomes important. Thus the β-plane assumption is relaxed in section 4, where a planetary geostrophic model is considered. In most of the development below, we are interested in the limit of weak viscosity and so will order the parameters such that

$$\delta_m \ll \delta_K \ll \delta_T = O(1), \tag{2.7}$$

and we will discuss the consequences of reversing the first inequality.

For comparison with the f-plane model of earlier studies, for example, Pedlosky (2003), it is useful to note the following equivalents:

$$E = \frac{A}{f_o L^2} = b\delta_m{}^3, \tag{2.8a}$$

$$S = \frac{L^2}{L_d{}^2}, \tag{2.8b}$$

$$\sigma = A/\kappa, \tag{2.8c}$$

$$E/\sigma S = b\delta_K, \quad \text{and} \tag{2.8d}$$

$$\gamma/f_o S = b/\delta_T. \tag{2.8e}$$

The first is the Ekman number, the second is the stratification parameter, and the third is the Prandtl number.

An additional boundary layer scale enters the problem and is familiar from the f-plane models. We define this scale as

$$\delta_h = (\sigma S)^{1/2} = (\delta_m{}^3/\delta_K)^{1/2}. \tag{2.9}$$

This is the scale for the hydrostatic layer (Pedlosky 2003). Its width is independent of β and in the f-plane models is the scale over which the strong vertical motions near the boundary occur. We will see the reemergence of this boundary layer with the same function in the β-plane model. It is important to note that in the f-plane models the characteristic vertical transport in the interior and in the boundary layers is $O(E/\sigma S) = b\delta_K$ and this gives us a useful point of comparison for the β-plane case where we will find vertical transports that are larger by a factor of δ_K^{-1}.

b. Boundary layer structure

Although it is not necessary in this rather simple model to rely on boundary layer methods to find explicit solutions, it is useful for understanding the structure of the solution to outline the boundary layer character of the motion. Since both diffusion and friction are considered to be small effects, over most of the basin the motion is governed by the geostrophic relations, leading to the Sverdrup vorticity balance and to a cross-isopycnal velocity determined by the departure of the interface height from θ. Departures from this balance will only occur in narrow regions near the basin boundaries.

For simplicity we will consider the case in which θ is a function only of latitude (y). Thus in the interior,

$$fu = \eta_y, \tag{2.10a}$$

$$f\upsilon = -\eta_x, \tag{2.10b}$$

$$u_x + \upsilon_y = 2w_i, \quad \text{and} \tag{2.10c}$$

$$w_i = \frac{b}{\delta_T}(\eta - \theta), \tag{2.10d}$$

leading to

$$b\upsilon = -2fw_i, \tag{2.11a}$$

which is the Sverdrup relation. Combining (2.11a) with (2.10b) and (2.10d) yields the governing equation for the interface height in the interior,

$$\frac{\partial \eta}{\partial x} - 2\frac{f^2}{\delta_T}\eta = -2\frac{f^2}{\delta_T}\theta(y), \tag{2.11b}$$

whose solution is

$$\eta_I = \theta + (N_e - \theta)e^{-2f^2(x_e - x)/\delta_T}, \tag{2.12a}$$

$$v_I = -2(N_e - \theta)\frac{f}{\delta_T}e^{-2f^2(x_e - x)/\delta_T}, \quad \text{and} \tag{2.12b}$$

$$w_{i_I} = \frac{b}{\delta_T}(N_e - \theta)e^{-2f^2(x_e - x)/\delta_T} = \frac{b}{\delta_T}(\eta - \theta). \tag{2.12c}$$

Here we have labeled the interior solution with a subscript I. The interior solution takes on a constant value for the interface height N_e on the eastern boundary to avoid a zonal geostrophic velocity normal to the boundary at x_e. The constant N_e is not determined to this point. Note that the interface height approaches the prescribed external cooling θ as the distance from the eastern boundary increases and so quenches exponentially the vertical motion. If the scale $\delta_T < x_e$, the interior downwelling and meridional velocity are limited to a region near the eastern boundary west of which the flow is zonal and the interface approaches θ.

For small b, f in the above equations can be replaced by unity. Note that the total upwelling in the interior of the basin at each latitude,

$$\int_0^{x_e} w_{iI}\, dx = \frac{b}{2}(N_e - \theta)(1 - e^{-2x_e/\delta_T}), \qquad (2.13)$$

where we have set, to lowest order, $f = 1$. As noted above, the vertical transport is $O(b)$ rather than $b\delta_K$ as on the f plane.

In the vicinity of the western boundary a boundary layer is required to satisfy, first of all, the condition of no normal flow. When $\delta_K \gg \delta_m$, that boundary layer is a thermal layer (indeed, in that parameter limit the Munk layer balances are not consistent and the Munk layer does not exist). The dependent variables in the boundary layer are correction functions to the interior flow and they vanish as the boundary layer independent variable $\xi = x/\delta_K$ grows large. The dependent variables for the correction functions are

$$(u_K, v_K, w_{i_K}, \eta_K) = \frac{U}{\delta_K}(\delta_K\tilde{u}, \tilde{v}, \tilde{w}, \delta_K\tilde{\eta}). \qquad (2.14)$$

Note that the meridional and vertical velocities are $O(\delta_K^{-1})$ larger than their interior values since the value of U will be fixed by canceling the interior zonal velocity with this boundary layer correction.

The equations governing the thermal diffusive layer can be shown to be

$$f\tilde{u} = \tilde{\eta}_y, \qquad (2.15a)$$

$$f\tilde{v} = -\tilde{\eta}_\xi, \qquad (2.15b)$$

$$\tilde{u}_\xi + \tilde{v}_y = 2\tilde{w}_i, \qquad (2.15c)$$

$$\tilde{w}_i = -b\tilde{\eta}_{\xi\xi}, \quad \text{and} \qquad (2.15d)$$

$$\Rightarrow 2\tilde{\eta}_{\xi\xi} + \tilde{\eta}_\xi = 0. \qquad (2.15e)$$

The solution to (2.15) that satisfies the normal flow condition on $x = 0$, equivalent in the quasigeostrophic limit to setting the interface height to N_e at $x = 0$, is

$$\tilde{\eta} = (N_e - \theta)(1 - e^{-2x_e/\delta_T})e^{-\xi/2} \quad \text{and} \qquad (2.16a)$$

$$\tilde{w}_i = -\frac{b}{4}(N_e - \theta)(1 - e^{-2x_e/\delta_T})e^{-\xi/2}, \qquad (2.16b)$$

while the other fields are immediately obtained from (2.15). It is important to note that at each latitude

$$W_I = \int_0^{x_e} w_{i_I}\, dx = \frac{b}{2}(N_e - \theta)(1 - e^{-2x_e/\delta_T}) = -W_K = -\delta_K\int_0^\infty w_K\, d\xi \qquad (2.17)$$

so that the total vertical *mass flux in the western boundary layer is equal and opposite to the interior's vertical mass flux*. If there is to be a net vertical mass flux it must arise in yet another, more narrow region of the flow. The balance of the interior and diffusion layer vertical transports follows directly from the fact that the meridional velocity is in Sverdrup balance in both the interior and diffusion layer, so the vertical and meridional velocities are linearly related. Since the net integrated meridional transport must balance at lowest order in quasigeostrophic theory, it follows that the net vertical transports must also balance.

In this parameter limit a thinner boundary layer whose scale is $\delta_h = (\delta_m^3/\delta_K)^{1/2}$ [see (2.9)] exists. Its width is independent of β and in the terminology of the f-plane models it is called the hydrostatic layer. Its function in the boundary layer construction of the solution is to bring the tangential velocity to zero at the boundary. In this narrow region the *corrections* to the composite solution thus far attained can be written

$$(u_h, v_h, w_h, \eta_h) = V\left(\delta_h\hat{u}, \hat{v}, b\frac{\delta_K}{\delta_h}\hat{w}, \delta_h\hat{\eta}\right), \qquad (2.18)$$

where the caret variables are functions of $s = x/\delta_h$. The caret variables satisfy

$$f\hat{v} = -\hat{\eta}_s, \qquad (2.19a)$$

$$f\hat{u} = \hat{\eta}_y + b\left(\frac{\delta_m}{\delta_h}\right)^3\hat{v}_{ss}, \qquad (2.19b)$$

$$2b\frac{\delta_K}{\delta_h}\hat{w} + b\hat{v} = b\frac{\delta_K}{\delta_h}\hat{v}_{sss}, \quad \text{and} \qquad (2.19c)$$

$$b\hat{w} = -b\hat{\eta}_{ss}. \qquad (2.19d)$$

Note that the parameter

$$b\frac{\delta_m^3}{\delta_h^3} = \frac{E}{(\sigma S)^{3/2}} \ll 1. \qquad (2.20)$$

It follows directly that satisfying the no-slip condition on v, which velocity is dominated by the contribution from the western boundary layer's diffusion solution (2.15), yields

$$w_h(s) = -\frac{b}{2^{1/2}\delta_h}(N_e - \theta)(1 - e^{-2x_e/\delta_T})e^{-2^{1/2}s}. \qquad (2.21)$$

It is important to note that the vertical velocity takes its largest values in this thinnest of all the layers, and that its total mass flux at each latitude is

$$W_h = \delta_h\int_0^\infty w_h\, ds = \frac{b}{2}(N_e - \theta)(1 - e^{-2x_e/\delta_T}) = -W_K = W_I. \qquad (2.22)$$

The total vertical mass flux in the hydrostatic layer is exactly equal to the interior's vertical transport and opposite to that of the diffusive boundary layer. The latter two cancel because the thermal balance in both layers balances the lateral diffusion of interface height (or buoyancy) against the vertical velocity. Since the no-slip condition (or equivalently an insulating condition) requires that the interface has zero slope in a direction normal to the wall, the integral of the sum of both boundary layers must vanish. We therefore have an alternation of vertical transport from region to region. The interior and the western boundary layer carrying the horizontal transport cancel their contributions to the vertical flux due to the Sverdrup balance and the quasigeostrophic condition that the net meridional mass flux vanish. The hydrostatic layer then remains as the only layer capable of carrying a net vertical mass flux and it does so in the narrowest of the boundary layer regions.

Furthermore, as we have noted in comparison with the *f*-plane models, the vertical transport is larger by a factor of δ_K^{-1} because the horizontal velocity in the western boundary current is amplified by this amount, and it is the reduction of this large meridional velocity to zero that drives the large vertical mass flux in that region's hydrostatic layer. Even though the hydrostatic layer has the same structure as on the *f* plane, the magnitude of its vertical velocity is greater on the β plane because the meridional velocity in the δ_K layer that it must bring to rest at the wall is larger. The effect of β has produced a western intensification of both meridional and vertical velocities and, in particular, localization of the net vertical mass flux to within a distance of δ_h of the western wall and so has indirectly affected the strength but not the structure of the hydrostatic layer.

On the northern and southern boundaries of the domain a similar double boundary layer structure occurs. However, as in homogeneous models, the layer necessary to close the lateral transport is wider than the boundary layer on the western boundary and consequently the vertical mass flux in the hydrostatic layer is less. In addition, for the same reasons as just described, the total vertical mass flux of the two northern boundary layers cancels and there is thus no *net* vertical transport in these layers, so we will not discuss them further for reasons of concision. A hydrostatic layer on the eastern boundary is also required to satisfy the no-slip condition there. Again, since the meridional velocity is small there, its contribution to the total flux is normally very much smaller than the western contribution.

To complete the solution the value of the interface height on the eastern boundary must be determined. This is accomplished by balancing the total vertical mass flux in the basin against a small $O(b)$ net outflow, ΔV. From the continuity equation,

$$\oint_C \mathbf{u}\cdot\mathbf{n}\, dl = 2\int_0^{L_y}\int_0^{x_e} w_i\, dx\, dy = b\Delta V. \quad (2.23)$$

The vertical velocity is related to the interface height by (2.5d), and carrying out the integral of (2.23) determines N_e in terms of the specified outflow. Note that this balance occurs at $O(b)$ and is higher order than the quasigeostrophic dynamics used here. In the appendix, a uniformly valid solution that avoids some of the boundary layer approximations is constructed to satisfy the no-normal-flow conditions on each boundary and is used to determine the hydrostatic layer contribution to the net vertical flux and yields a determination of N_e as shown in (A.9).

It is interesting to note that, if the analysis is repeated for a model in which there is no lateral diffusion of buoyancy, that is, if $\delta_K = 0$, or equivalently, if $\delta_K \ll \delta_m$, the structure of the solution changes drastically. In that case the boundary conditions of no normal flow and no slip are satisfied by a Munk layer on each wall. Since the velocity along the boundary is in geostrophic balance, the total interface height deviation in the Munk layer never exceeds that of the interior. The vertical velocity from (2.5d) is $O(b\delta_T^{-1})$ so that the total vertical transport in the Munk layer is $O(b\delta_m/\delta_T)$ and, so, is much *smaller* than the interior transport. Whereas we have found strong vertical velocities in the hydrostatic layer carrying the net vertical transport, a model that ignores the lateral diffusion of buoyancy would have its major vertical mass flux in the interior. Note that the total transport in both cases is the same but the structure of the vertical motion is strikingly different.

3. Results of the quasigeostrophic analytical model

We consider the circulation forced by a linear increase in the externally imposed interface height corresponding, roughly speaking, to a decreasing surface temperature as the model's forcing. That is, we take $\theta = \theta_o(y/L_y)$. We use the results of the appendix to first calculate the interface height on the eastern boundary as a function of the small $O(b)$ inflow into the basin. Using (A.9), Fig. 2 shows the relation between ΔV and N_e. Note that, generally speaking, if we arbitrarily assumed that the interface height on the eastern boundary were undisturbed, that is, zero, this would require a small *inflow*. In general we can *specify* either the inflow or the interface height (temperature) on the eastern boundary and the consistency between them is determined by the mass flux balance (2.23), which can be

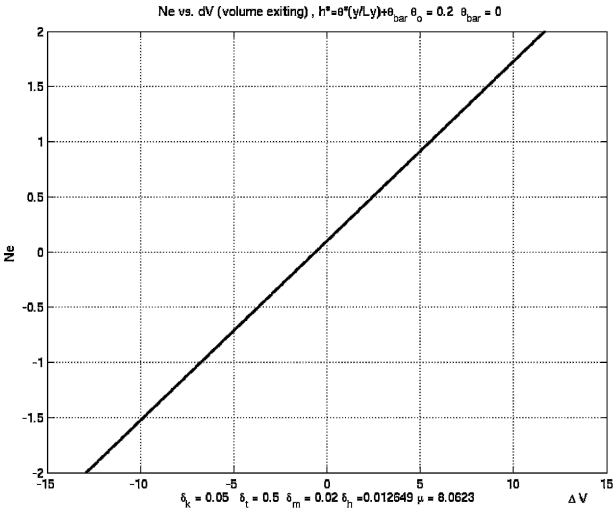

FIG. 2. The relation between ΔV and N_e as obtained from (A.9) for the parameter values $\delta_m = 0.02$, $\delta_K = 0.05$, $\delta_T = 0.25$, and $\theta_o = 0.2$, while $x_e = 1$ and $L_y = 4$.

shown for quasigeostrophic dynamics to be equivalent to a Kelvin circulation integral for the basin as a whole. One of the two must be specified if less than the full world's ocean is considered.

Figure 3 shows the interface height for the parameters of Fig. 2 as given by the solution in the appendix. An *inflow* mass flux = 0.50 (so that $\Delta V = -0.5$) has been specified. The strong recirculation region near the northern boundary of the basin is a consequence of the linearly increasing forcing, and the solution of the appendix accounts for the boundary layer structure in that region. Note that for the fairly small values of δ_T and δ_K the meridional motion is confined to regions near the eastern and western boundaries. The baroclinic meridional flow in the eastern (interior) part of the basin is northward, reflecting the fact that there is a net inflow. A net inflow requires a net sinking and that, in turn, requires a net sinking in the interior. That vortex tube stretching (shrinking) for the upper (lower) layer produces a positive meridional baroclinic velocity. However, the largest vertical velocity occurs in the hydrostatic layer, in particular the layer adjacent to the western boundary. Figure 4 shows the profile of the vertical velocity at the midlatitude of the basin, $y = L_y/2$. For these parameter values the vertical velocity in the vicinity of the eastern boundary is also significant if rather smaller than its western counterpart. This is due to the relatively small value of δ_T, which has enhanced the meridional velocity in the vicinity of the eastern boundary. If that scale is increased so that a baroclinic Rossby wave can cross the basin without being completely dissipated (e.g., for $\delta_T = 2$), the results show a greater east–west asymmetry. Figures 5 and 6 show the interface height and vertical velocity for the same parameter settings as in Fig. 3 except that now $\delta_T = 2$. The weaker dissipation allows the Rossby wave signal to fill the interior, giving rise to stronger meridional and vertical motions there although, as seen in Figs. 4 and 6, the interior velocities are always weak compared to the boundary layer vertical velocity. The flow in the interior is now largely meridional and the weaker concen-

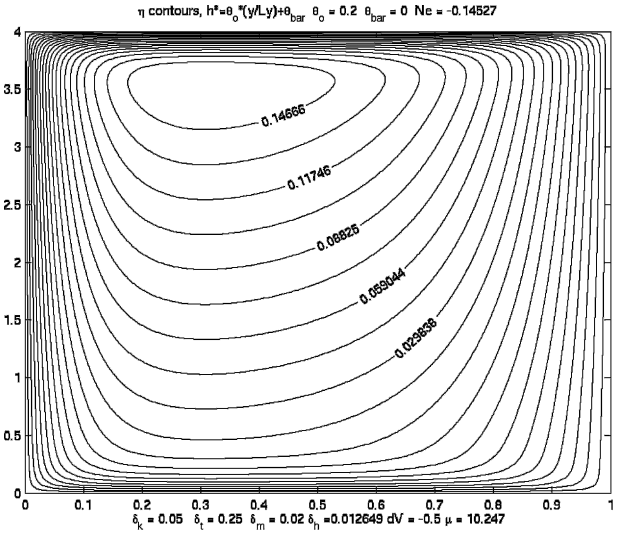

FIG. 3. A contour plot of the interface displacement obtained from the solution of the appendix for the parameter settings of Fig. 2 and the specification of $b\Delta V = -0.05$, i.e., a net *inflow*. Note the strongly zonal character of the flow away from boundaries.

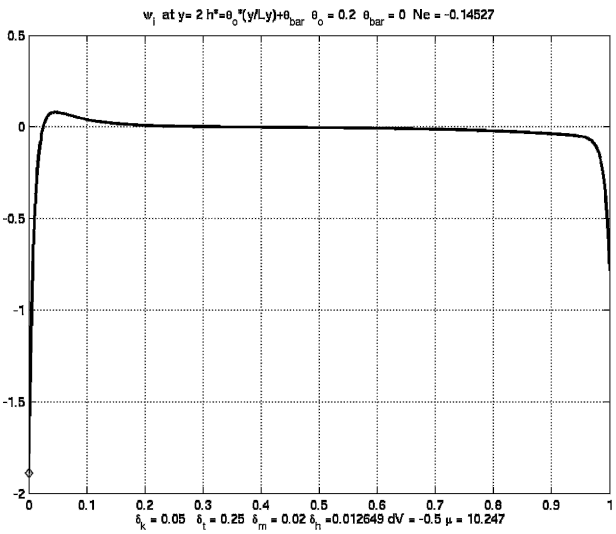

FIG. 4. The vertical velocity as a functions of x at $y = L_y/2$ for the same parameter settings as Fig. 3. Note the concentration of the vertical velocity near the boundaries, especially the western boundary.

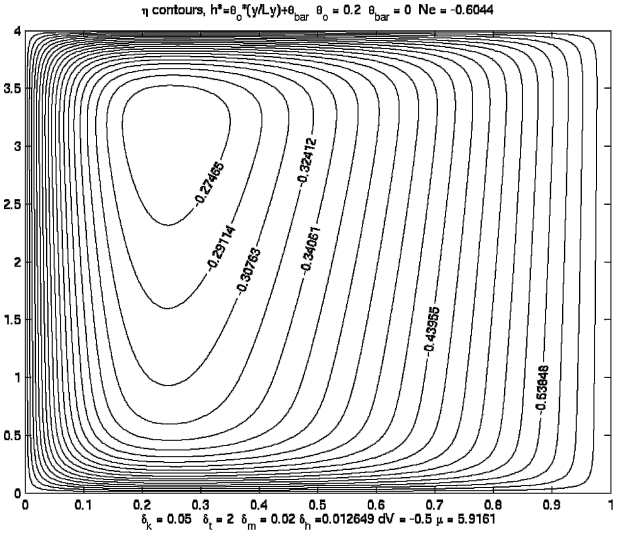

FIG. 5. A contour plot of interface displacement for the parameter settings of Fig. 3, but for $\delta_T = 2$. The horizontal circulation is much more meridional.

tration of the meridional velocity near the eastern boundary leads to a much weaker downwelling near $x = x_e$. The downwelling is now almost entirely concentrated at the western boundary. Note that there is a weak north–south asymmetry to the vertical velocity; it is larger in the north since v is larger there. This asymmetry is even larger in the planetary geostrophic solutions described below.

If we arbitrarily close off the basin so that there is no flow entering or leaving, we then have $\Delta V = 0$. Now there can be no net sinking over the basin and so no net sinking in the interior. The flow responds by producing counterrotating gyres: clockwise in the south and counterclockwise in the northern half of the gyre as shown in Fig. 7. This leads to upwelling in the southern gyre and sinking in the northern gyre to yield a detailed balance of no net vertical mass flux. Figure 8 shows the profiles of vertical velocity at a latitude in the center of the southern gyre, that is, at $y = L_y/4$. The strongest vertical velocity is, again, along the western boundary where the hydrostatic layer carries the net vertical mass flux of the southern gyre. The northern gyre is the mirror image of the southern one and the profiles have the same shape but are reversed in sign. It is striking how sensitive the overall circulation is to an $O(b)$ net inflow. The quasigeostrophic circulation at $O(1)$ is completely altered in its structure. This is not surprising when we realize that the small inflow produces a net influx of potential vorticity, absent of which the circulation must change its structure to produce no net potential vorticity dissipation in the basin since the *vertical* velocity is incapable of changing the net potential vorticity. Note also that the inflow enters only in an integrated condition on the mass balance. The $O(1)$ circulation would have the *same form regardless of the location of the inflow,* at least in quasigeostrophic theory.

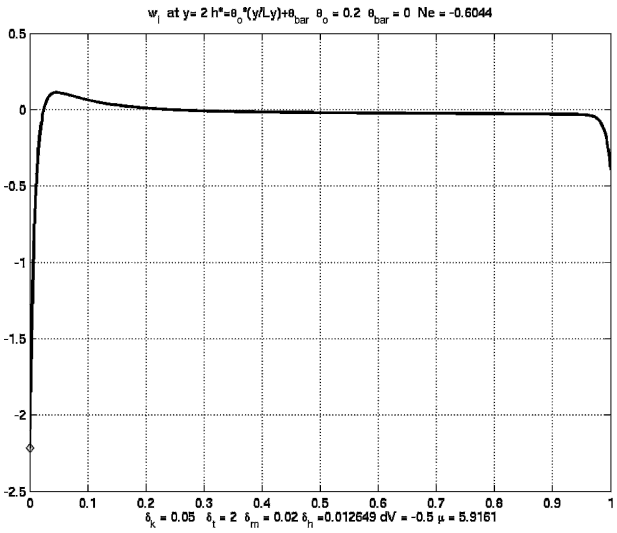

FIG. 6. As in Fig. 4, but for $\delta_T = 2$.

4. Higher-order effects

a. Planetary geostrophy

The planetary geostrophic (PG) approximation allows us to extend several of the limitations of the quasi-

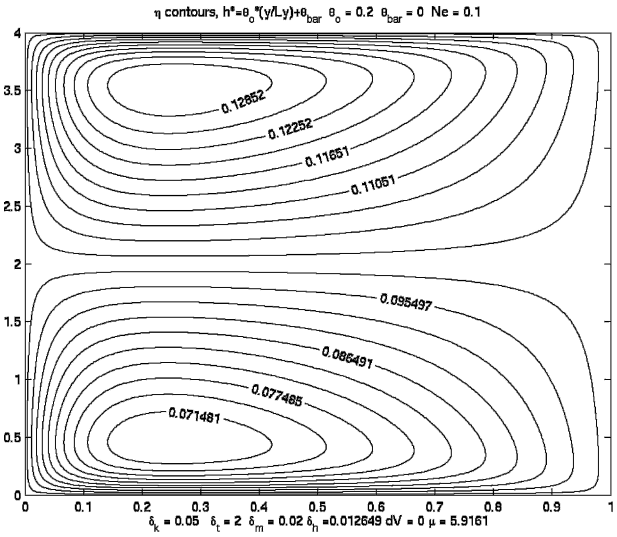

FIG. 7. The interface displacement for the parameters of Fig. 5 except that now $\Delta V = 0$. The circulation has split into two counterrotating gyres and the downwelling in the northern part of the basin exactly balances the upwelling in the southern part.

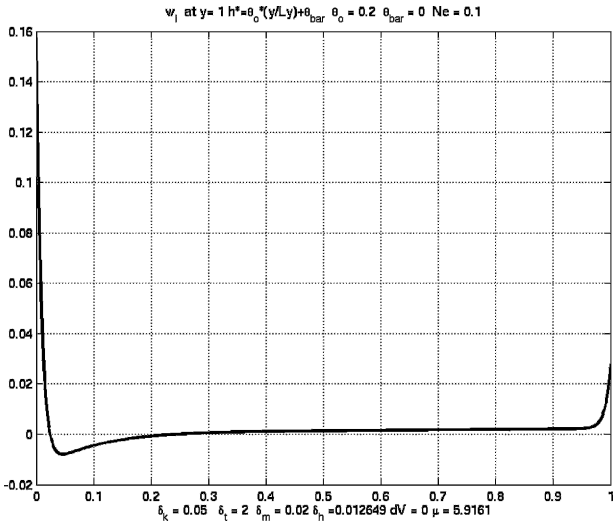

FIG. 8. Profiles of interface height and vertical velocity for the parameters of Fig. 7 at a latitude $y = L_y/4$, i.e., at the midpoint of the southern gyre. Note the strong upwelling on the western boundary in the hydrostatic layer.

geostrophic equations in the previous section while still providing analytic solutions (although they must be integrated numerically). In particular, for PG dynamics, the Rossby wave phase speed is a function of latitude and the variation in the Coriolis parameter as measured by b can be $O(1)$ over the domain. A more subtle point is that the subgrid-scale parameterizations in the PG equations are derived from the total circulation, not just the zeroth-order circulation. Since we are interested in the effect of β on basin scales, it is of interest to see how these changes affect the conclusions based on QG dynamics.

The solution procedure follows closely that of Spall (2003b), so only a brief outline is provided here. The model is analogous to the QG model in the previous section. The fluid consists of two layers of slightly different density and is forced by a relaxation of the interface height toward $h(y)$ with time scale γ^{-1}. The solution for the interface height comprises this specified interface displacement $h(y)$ and boundary layers that are required in order to satisfy the no-slip and no-normal-flow boundary conditions on the eastern and western boundaries. We do not explicitly consider the northern and southern boundary layers because, as discussed previously, it is expected that there will be little net vertical motion there. For the cases considered here, the forcing is chosen to drive a uniform eastward flow of amplitude U, for example, $\partial h/\partial y = -U(1+by)$. The boundary layer structures are determined by solving the nondimensional vorticity equation for the nondimensional perturbation pressure P, which is related to the dimensional interface displacement η by $P = g'\eta/f_0UL$:

$$\delta_m^3 P_{xxxx} - (1+by)^2\delta_K P_{xx} - P_x + (1+by)^2\delta_T^{-1}P = 0. \tag{4.1}$$

The parameters are as previously defined, and the vertical velocity is due to both a restoring of the interface and lateral diffusion, as in (2.5d). It is assumed that the perturbation pressure P decays exponentially away from the eastern and western boundaries, for example, $P \propto e^{ikx}$. This results in a fourth-order equation with four roots k_1, k_2, k_3, and k_4:

$$\delta_m^3 k^4 + (1+by)^2\delta_K k^2 - ik + (1+by)^2\delta_T^{-1} = 0. \tag{4.2}$$

There are two roots with negative imaginary components that decay away from the eastern boundary (k_1, k_2,) and two roots with positive imaginary components that decay away from the western boundary (k_3, k_4).

The solution for the nondimensional upper-layer thickness may be written as (see Spall 2003b for details)

$$\eta(x,y) = -U(y + 0.5\beta y^2) + A(y)[e^{ik_1(x-x_e)} - (k_1/k_2)e^{ik_2(x-x_e)}] + B(y)[e^{ik_3x} - (k_3/k_4)e^{ik_4x}]. \tag{4.3}$$

The functions $A(y)$ and $B(y)$ in (4.3) determine the interface variation along the eastern and western boundaries. The no-normal-flow boundary condition at the eastern boundary results in the following equation for $A(y)$:

$$A_y = \left(\frac{C_1}{1+by} + C_3\right)A + C_2U(1+by). \tag{4.4}$$

The coefficients are defined as

$$C_1 = ik_1k_2(k_1+k_2)E, \tag{4.5a}$$

$$C_2 = \frac{k_2}{k_2-k_1}, \quad \text{and} \tag{4.5b}$$

$$C_3 = \frac{\partial(k_1/k_2)}{\partial y}C_2. \tag{4.5c}$$

An equation similar to (4.4) is derived for the amplitude $B(y)$ along the western boundary using the roots k_3 and k_4.

The equations are solved by initially assuming an interface height at some point on the boundary, say the southeast corner of the domain. Equation (4.4) is integrated northward along the eastern boundary, keeping in mind that C_1, C_2, C_3, k_1, and k_2 are functions of y because the Rossby wave phase speed is a function of latitude in PG dynamics. It is assumed that the net

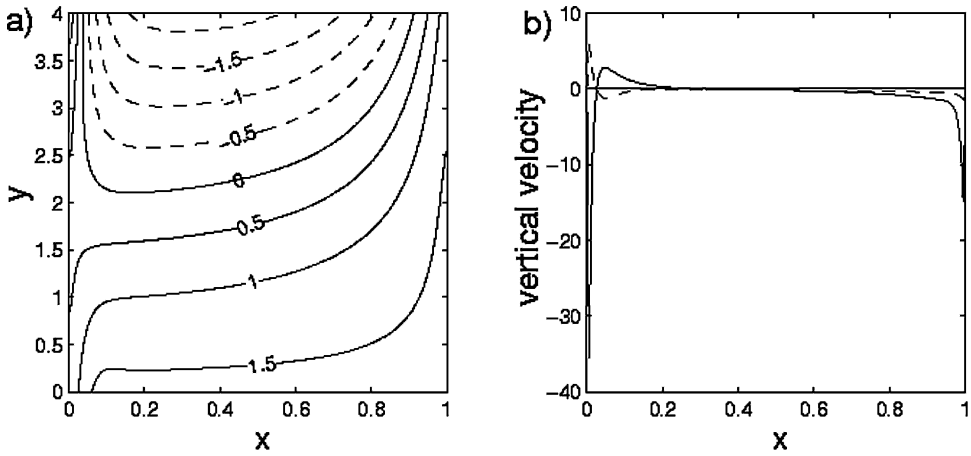

FIG. 9. Solution for the planetary geostrophic equations with boundary layer thicknesses: $\delta_m = 0.02$, $\delta_K = 0.05$, $\delta_T = 0.25$, and $b = 0.2$. The model is forced by a relaxation of the upper-layer thickness that produces a uniform eastward flow in the upper layer. (a) Nondimensional upper-layer thickness, and (b) vertical velocity at $y = 3$ (solid line) and $y = 1$ (dashed line).

vertical motion near the northern boundary is small so that the interface height is the same on the boundary in the northwest corner as it is on the boundary in the northeast corner. The equation analogous to (4.4) for the western boundary is then integrated southward to the southwest corner of the domain. Once the functions $A(y)$ and $B(y)$ are known, the solution is obtained from (4.3). In general, the pressure anomaly at the southwest corner will not be equal to the pressure anomaly at the southeast corner. The difference drives a geostrophic meridional flow through the southern boundary, the net inflow or outflow into the basin ΔV from the previous section. One could instead specify this inflow and iterate the initial guess for the pressure in the southeast corner until the inflow through the southern boundary exactly balanced the desired net flow into the basin.

We consider the case of a decreasing upper-layer thickness toward the north, as in the previous QG solutions. The southern boundary is treated as open and able to provide whatever meridional transport is required by the PG solution within the basin. The intent here is to represent a basin subject to a net cooling that is closed to the north and open to the south. The justification for specifying the pressure anomaly in the southeast corner is that the thickness anomaly here is determined by Kelvin waves propagating cyclonically into the basin from the south, and thus the pressure (or upper-layer thickness) in this southeast corner is not determined from within the basin. It is assumed here that the upper-layer thickness in the southeast corner is equal to $h(y = y_s)$, the thickness to which the upper layer is being restored at the southern latitude of the model domain.

The interface displacement for a case analogous to that in Fig. 2 is shown in Fig. 9a. The parameters are the same as for the QG case except for a slightly greater value of b; that is, $\delta_m = 0.02$, $\delta_K = 0.05$, $\delta_T = 0.25$, and $b = 0.2$. The basic circulation looks much like the QG solution. The flow is dominated by a large-scale cyclonic circulation with strong meridional flows near the eastern and western boundaries. The pressure contours in the interior get closer together as one moves north because the model is forced with a uniform eastward flow and the Coriolis parameter increases with latitude. The pressure contours intersect the eastern and western boundaries as the higher-order ageostrophic circulation is explicitly represented in the pressure field, whereas it is not included in the QG streamfunction (although it can be derived). The downwelling along the eastern boundary is evident by the pressure contour intersecting the boundary. The major difference from the QG solution is the presence of northward flow across the southern boundary in the southwest corner of the domain. This provides the net mass flux into the basin that is eventually downwelled. This inflow is balanced by a southward flow along the western boundary in the deep layer As a result of this inflow, there is now a stagnation point along the western boundary. The strength of this northward flow, and location of the stagnation point, depends on the change in pressure along the boundary. The inflow increases, and the stagnation point moves northward, with increasing Ekman number.

One can show through solutions to (4.2) that the same basic boundary layers discussed for the QG solutions are present in the PG solutions. The net downwelling takes place near the western boundary and, to a

lesser extent, near the eastern boundary in the narrow δ_h layers. The Sverdrup upwelling and downwelling support the large-scale cyclonic circulation. The vertical velocity is shown in Fig. 9b at $y = 3$ (solid line) and at $y = 1$ (dashed line). The vertical motions are still largest near the boundaries, but there is now a significant north–south asymmetry. The downwelling is largest in the northern basin near the western boundary and somewhat smaller near the eastern boundary. However, the vertical motion near the southwestern boundary is now upwelling in the western δ_h layer and downwelling in the broader δ_K western boundary layer. This is because, when the higher-order circulation is taken into account, the flow near the western boundary is no longer everywhere to the south but actually changes direction toward the north in the southern basin. This effect is not included in the QG model because the upwelling is parameterized using the QG streamfunction only.

Provided the pressure is continuous along the boundary, the net inflow or outflow into each of the layers in the basin occurs through the southern open boundary in the form of a western boundary current. The net transport into the basin goes through a basin-scale cyclonic recirculation before it ultimately downwells near the boundary in the northwest portion of the domain. If the layer thickness at the southeast corner is chosen such that there is no mass flux through the southern boundary, the two-gyre circulation found in the quasi-geostrophic model (Fig. 7) is reproduced. It is important to note that the extension from QG to PG dynamics has not altered the basic result, that the net vertical motion is concentrated within narrow boundary layers of width δ_h along the western boundary and that the large-scale circulation remains very sensitive to the net mass flux into the basin.

b. Primitive equation numerical model

A two-layer version of the MICOM isopcynal primitive equation model (Bleck et al. 1992) has been configured similar to the previous QG and PG formulations. This allows us to test the robustness of the basic results from the previous analytic models in the presence of more complete physics, including nonlinearities, instabilities, and eddy fluxes. The model domain extends 2000 km in the zonal direction and 4000 km in the meridional direction and has a uniform horizontal resolution of 10 km. The model is initialized at rest with two layers each of 500-m thickness. The model is forced by a source of 10×10^6 m^3 s^{-1} that converts layer-2 water into layer-1 water in a narrow strip 10 km wide extending from $x = 0$ to $x = 200$ km along the southern boundary of the model domain. The upper-layer thickness is restored toward a linear profile that is 600 m at the southern boundary of the model and 400 m at the northern boundary. The relevant dimensional boundary layer thicknesses are $\delta_m = 15$ km, $\delta_K = 30$ km, and $\delta_T = 500$ km (nondimensional values are $\delta_m = 0.0075$, $\delta_K = 0.015$, and $\delta_T = 0.25$). The diffusive boundary layers are very narrow in order to allow instabilities and eddies to develop in the numerical model. The stratification is chosen such that the internal deformation radius at the midlatitude of the basin is 28 km. The Coriolis parameter varies from 0.8×10^{-4} s^{-1} at the southern boundary to 1.2×10^{-4} s^{-1} at the northern boundary, giving the nondimensional parameter $b = 0.2$. The model is initialized at rest and integrated for a period of 5 yr.

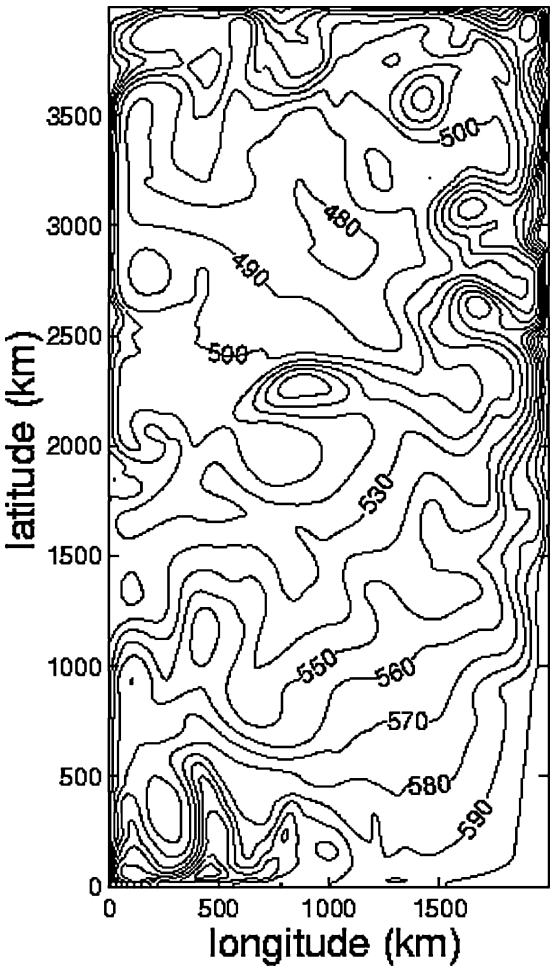

FIG. 10. Upper-layer thickness on day 820 from a two-layer calculation using the MICOM primitive equation model (contour interval is 10 m). The large-scale cyclonic circulation is dominated by synoptic eddies in the interior and strong boundary currents.

The upper-layer thickness on day 820 reflects the imposed north–south gradient (Fig. 10), but also shows strong deviations due to nonlinearities and time-depen-

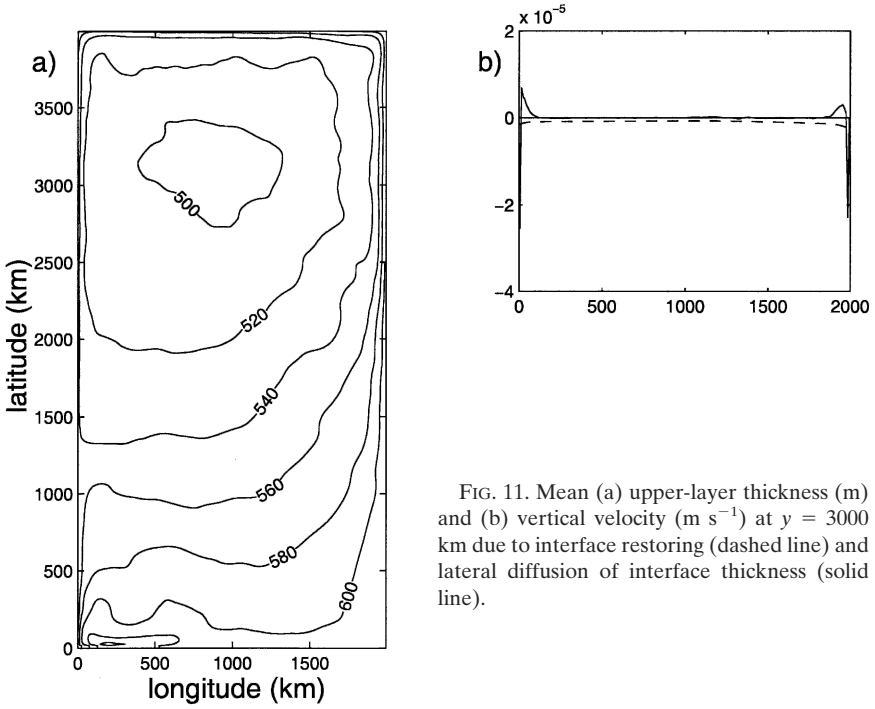

FIG. 11. Mean (a) upper-layer thickness (m) and (b) vertical velocity (m s^{-1}) at $y = 3000$ km due to interface restoring (dashed line) and lateral diffusion of interface thickness (solid line).

dent eddies. In particular, the northward flow in the interior of the eastern basin is strongly unstable and produces many eddies. The eddies carry heat away from the eastern boundary into the interior where they are eroded by the interface restoring term and, to a lesser extent, lateral diffusion. Eddies are also formed from each of the other boundary currents and from the source region in the southwest corner of the domain.

The mean upper-layer thickness calculated over the final three years of integration looks similar to that predicted by the QG and PG theories (Fig. 11a). There is an eastward flow over most of the interior, which turns toward the north near the eastern boundary. Much of this northward flow recirculates cyclonically in the northern half of the basin. There is also a stagnation point located near $y = 1300$ km along the western boundary, in general agreement with the PG theory. The northern portion of the domain is much warmer (thicker upper layer thickness) than is predicted by linear theory. The baroclinic eddies shed from the eastern and northern boundary currents are more effective at transporting heat into the interior than are baroclinic Rossby waves (the only mechanism in linear theory) at this latitude (LaCasce and Pedlosky 2004).

The vertical velocity at $y = 3000$ km is shown as a function of longitude in Fig. 11b. The lateral diffusion term clearly shows the boundary layer structure predicted by linear theory. The downwelling is most intense in a very narrow boundary layer along the western boundary, and there is also a region of strong, narrow downwelling along the eastern boundary. The eastern boundary current is stronger and narrower in this nonlinear calculation than predicted by linear theory, so the vertical motion, required to satisfy the no-slip boundary condition, is also stronger than predicted by linear theory. Outside of these narrow downwelling regions we find somewhat broader regions of weaker upwelling, the δ_K boundary layers. The numerical model also produces weak downwelling throughout the interior due to the interfacial restoring term. This does not show the exponential decay away from the eastern boundary that would be found for a steady solution in which heat transport is carried by first-mode baroclinic Rossby waves, and reflects the efficiency of the zonal eddy heat transport in this model. Note that, even though the mesoscale eddy field is dominant over the Laplacian diffusion of heat in the interior, the δ_h boundary layer is still required to satisfy the lateral boundary conditions and ultimately plays the same role in driving the vertical motion as in the linear theory.

5. Summary and discussion

We have examined simple two-layer models of the buoyancy-driven circulation in a ocean basin of large enough extent for the β effect to be important although in the analytical theory we have assumed it small enough to allow the use of the β plane and, in one model, the quasigeostrophic approximation.

The major result of our study is that when processes that produce lateral transport of buoyancy are included, in the present case modeled analytically by a lateral diffusion of interface height or with baroclinic eddy processes in the numerical model, the largest vertical motions occur in very narrow boundary layer regions near the western boundary of the basin. The western intensification of the horizontal circulation has its counterpart in the western intensification of the vertical circulation. The effect of β on the vertical circulation is an indirect but profound one. By intensifying the meridional velocity in the western boundary layer that closes the horizontal circulation, the induced vertical velocity in the hydrostatic layer is greatly increased by an amount δ_K^{-1}. The lateral scale of this region is unaltered by β and remains on the order of $(A/\kappa)^{1/2}L_d$ as on an f plane. That is, it is still the deformation radius multiplied by the square root of the turbulent Prandtl number. Thus the net downwelling of the meridional overturning circulation depends on turbulent mixing processes near boundaries on scales smaller than the mesoscale. Resolving such small scales is often a difficulty in climate models and we are led to wonder whether the inability to do so can have serious consequences for the circulation as a whole. Ignoring such processes may not affect the net sinking for, as we saw, a model with no lateral diffusion predicts the same net sinking, but one broadly distributed over the interior rather than concentrated near the boundary. In more complex models than the one that we have considered here it seems likely that the structure of the sinking, as well as its overall total, would be important for the dynamics of the vertical and meridional circulation. See, for example, LaCasce (2004) for a discussion of a continuously stratified model with spatially variable mixing coefficients. In any case, it once more illustrates a general point that has been suggested by earlier studies—namely, that broad thermodynamic surface forcing can lead to intense, narrow zones of vertical motion near the basin boundaries.

Acknowledgments. This research was supported in part by grants from the National Science Foundation OCE-9901654 (JP) and OCE-0240978, and Office of Naval Research Grant N00014-03-0338 (MAS).

APPENDIX

Uniformly Valid Solution

In the parameter limit $\delta_m \ll \delta_K$ a uniformly valid solution for all δ_T/δ_K can be found. In that limit the interface height satisfies

$$2\delta_K\nabla^2\eta + \eta_x - 2\eta/\delta_T = -2\theta/\delta_T. \tag{A.1}$$

For concreteness, a forcing that is linear in y will be considered so that

$$\theta = \bar{\theta} + \theta_o(y/L_y). \tag{A.2}$$

A solution that satisfies the condition that η be a constant on $x = 0$ and $x = x_e$ can be found as

$$\eta_p = \theta + (N_e - \theta)\left[e^{-(x-x_e)/4\delta_K}\frac{\sinh\mu x}{\sinh\mu x_e} - e^{-x/4\delta_K}\frac{\sinh\mu(x-x_e)}{\sinh\mu x_e}\right]. \tag{A.3}$$

Here

$$\mu = \left(\frac{1}{16\delta_K^2} + \frac{1}{\delta_T\delta_K}\right)^{1/2}.$$

In this parameter regime the meridional velocity is geostrophic and the vertical velocity is in Sverdrup balance with v so that both may be easily found derived from (A.3).

To satisfy the no-normal-flow condition at $y = 0$ and $y = L_y$ an additional solution must be added in the form

$$\eta_h = e^{-x/4\delta_K}\Phi(x, y) \quad \text{and} \tag{A.4a}$$

$$\Rightarrow \nabla^2\Phi - \mu^2\Phi = 0. \tag{A.4b}$$

The solution that satisfies the boundary conditions on $y = 0$ and $y = L_y$ is

$$\Phi = \sum_{n=1}\left[A_n\frac{\sinh\alpha_n y}{\sinh\alpha_n L_y} + B_n\frac{\sinh\alpha_n(y-L_y)}{\sinh\alpha_n L_y}\right]\sin n\pi x/x_e, \tag{A.5a}$$

$$A_n = \frac{2}{x_e}\frac{n\pi}{x_e}[1-(-1)^n e^{x_e/4\delta_K}] \times\left[\frac{\mu^2 - 1/16\delta_K^2}{\left(\frac{n^2\pi^2}{x_e^2}+\frac{1}{16\delta_K^2}\right)\left(\frac{n^2\pi^2}{x_e^2}+\mu^2\right)}\right][N_e - \theta(L_y)], \tag{A.5b}$$

$$B_n = \frac{2}{x_e}\frac{n\pi}{x_e}[1-(-1)^n e^{x_e/4\delta_K}] \times\left[\frac{\mu^2 - 1/16\delta_K^2}{\left(\frac{n^2\pi^2}{x_e^2}+\frac{1}{16\delta_K^2}\right)\left(\frac{n^2\pi^2}{x_e^2}+\mu^2\right)}\right][N_e - \theta(0)], \tag{A.5c}$$

and

$$\alpha_n = \left(\frac{n^2\pi^2}{x_e^{\,2}} + \frac{1}{16\delta_k^2} + \frac{1}{\delta_T\delta_K}\right)^{1/2} \tag{A.5d}$$

so that

$$\eta = \eta_p + \eta_h. \tag{A.6}$$

Using (A.6) and the geostrophic relation for v it is then possible to calculate v at $x = 0$ and use the hydrostatic layer on $x = 0$ (2.19) to find the vertical velocity in the hydrostatic layer and its accompanying vertical velocity. After some algebra it follows that the vertical velocity in the western hydrostatic layer is

$$w_h = -\frac{2^{1/2}b}{\delta_h}(N_e - \theta)e^{-2^{1/2}s} \times \left(\frac{\mu\delta_K e^{x_e/4\delta_K}}{\sinh\mu x_e} - \frac{1}{4} - \mu\delta_K \coth\mu x_e\right), \tag{A.7a}$$

where $s = x/\delta_h$.

A similar calculation for the weaker hydrostatic layer at $x = x_e$ yields a vertical velocity

$$w_{he} = -\frac{2^{1/2}b}{\delta_h} e^{-2^{1/2}s_e}(N_e - \theta) \times \left(\frac{1}{4} + \frac{\mu\delta_K}{\sinh\mu\delta_K} - \mu\delta_K \coth\mu x_e\right), \tag{A.7b}$$

where $s_e = (x_e - x)/\delta_h$. Integrating each layer in x and y yields the net total upwelling:

$$\iint_{\text{bdy layers}} w_i\, dx\, dy = -b[(N_e - \overline{\theta})L_y + \theta_o L_y/2]2\mu\delta_K \times \left(\frac{\cosh x_e/4\delta_K}{\sinh\mu x_e} - \coth\mu x_e\right). \tag{A.8}$$

If this is used to balanced the specified $O(b)$ outflow from the basin, we obtain

$$\Delta V = -2[(N_e - \overline{\theta})L_y + \theta_o L_y/2]2\mu\delta_K \times \left(\frac{\cosh x_e/4\delta_K}{\sinh\mu x_e} - \coth\mu x_e\right). \tag{A.9}$$

REFERENCES

Bleck, R., C. Rooth, D. Hu, and L. T. Smith, 1992: Salinity-driven thermocline transients in a wind- and thermohaline-forced isopycnic coordinate model of the North Atlantic. *J. Phys. Oceanogr.,* **22,** 1486–1505.

Gent, P. R., and J. C. McWilliams, 1990: Isopycnal mixing in ocean circulation models. *J. Phys. Oceanogr.,* **20,** 150–155.

Gill, A. E., 1982: *Atmosphere–Ocean Dynamics*. Academic Press, 662 pp.

Huck, T., A. J. Weaver, and A. Colin de Verdiere, 1999: On the influence of the parameterization of lateral boundary layers on the thermohaline circulation in coarse-resolution ocean models. *J. Mar. Res.,* **57,** 387–426.

LaCasce, J., 2004: Diffusivity and viscosity dependence in the linear thermocline. *J. Mar. Res.,* **62,** 742–769.

——, and J. Pedlosky, 2004: The instability of Rossby basin modes and the oceanic eddy field. *J. Phys. Oceanogr.,* **34,** 2027–2041.

Marotzke, J., 1997: Boundary mixing and the dynamics of three-dimensional thermohaline circulations. *J. Phys. Oceanogr.,* **27,** 1713–1728.

Pedlosky, J., 2003: Thermally driven circulations in small ocean basins. *J. Phys. Oceanogr.,* **33,** 2333–2340.

Samelson, R., 1998: Large-scale circulation with locally enhanced vertical mixing. *J. Phys. Oceanogr.,* **28,** 712–726.

Spall, M. A., 2003a: On the thermohaline circulation in flat bottom marginal seas. *J. Mar. Res.,* **61,** 1–25.

——, 2003b: Islands in zonal flow. *J. Phys. Oceanogr.,* **33,** 2689–2701.

——, 2004: Boundary currents and water mass transformation in marginal seas. *J. Phys. Oceanogr.,* **34,** 1197–1213.